Journal of Materials Chemistry A

Accepted Manuscript

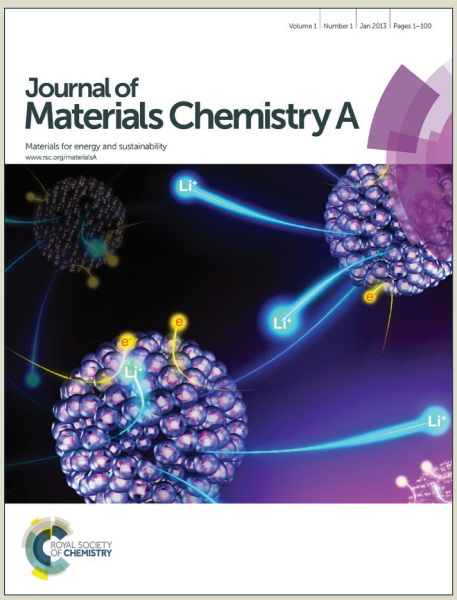

ROYAL SOCIETY OF CHEMISTRY

www.rsc.org/materialsA

Journal Name

RSCPublishing

ARTICLE

The Use of Time Resolved Aerosol Assisted Chemical Vapour Deposition in Mapping Metal Oxide Thin Film Growth and Fine Tuning Functional Properties

Cite this: DOI: 10.1039/x0xx00000x

Received ooth January 2012,
Accepted ooth January 2012

DOI: 10.1039/x0xx00000x

www.rsc.org/

Nicholas P. Chadwick[a], Sanjayan Sathasivam[ab], Salem M. Bawaked[c], Mohamed Mokhtar[c], Shaeel A. Althabaiti[c], Sulaiman N. Basahel[c], Ivan P. Parkin[a] and Claire J. Carmalt[a*]

Time resolved analysis of a thin film has allowed, for the first time, analysis of how thin film growth occurs and changes over time by aerosol assisted CVD. This method has also allowed tuning of the materials functional properties. In this report a hydrophobic and highly photocatalytic TiO_2/ SnO_2 system is studied, which exhibits surface segregation of SnO_2 and thus the novel formation of a natural hetero-junction charge transfer system. The time resolved samples were investigated by a variety of methods. The films were characterised by X-ray diffraction (XRD), X-ray photoelectron spectroscopy (XPS), scanning electron microscopy (SEM) and Ultraviolet- visible absorption spectroscopy (UV-Vis). Functional properties were investigated by photo-activity measurements and water contact angles before and after UV irradiation. The generation of representative samples at different times during the deposition sequence permitted changes in crystal structure, relative concentrations of atoms, and surface morphology to be linked intrinsically to changes in functional properties.

Introduction

Titanium dioxide is a widely studied photo-catalyst.[1–4] It is reported to be a material capable of use in environmental remediation strategies for the solar detoxification and cleaning of surfaces and water.[5–8] However, efficient electron hole recombination processes reduce the ability of titanium dioxide to carry out surface catalysis redox reactions.[9] Strategies to combat these processes have been employed in the form of dopants which trap electrons upon photo excitation and increase the lifetime of holes so as to allow more efficient surface redox reactions by increasing exciton lifetime. Many synthesis methods for forming doped TiO_2 exist[10–14] and one of particular interest is Aerosol Assisted Chemical Vapour Deposition (AACVD).[15–20]

AACVD is a flexible and highly advantageous technique for the production of metal oxide thin films of technological interest such as, SnO_2, TiO_2 and ZnO.[16,21,22] The ability of AACVD to produce a wide range of materials is attributed to its ability to utilise precursors previously inaccessible for other CVD methods. By dissolving a precursor into a solvent and aerosolising the solvent, use of a precursor is solely dependent upon finding a solvent in which it will dissolve. This conveys upon AACVD a degree of flexibility not found in other CVD techniques where volatile precursors are a prerequisite.

Previous work has centred on tin doped TiO_2[23] which exhibits high stability and high rates of photocatalysis. Ponja et *al* has published work detailing the production of a surface segregated titanium dioxide composite material by AACVD, consisting of a tin doped anatase TiO_2 layer with a surface layer of cassiterite SnO_2 which exhibits novel surface morphology, hydrophobicity and photocatalysis a magnitude better than an industry standard Pilkington Activ™.[24] The enhanced photo-activity was attributed to the natural formation of hetero-junction charge transfer scheme where TiO_2 based photoelectrons are sequestered by SnO_2 promoting the lifetime of holes and electrons alike. This echoes previous work where tin was found to surface segregate after incorporation into a TiO_2 matrix.[25] With this in mind it was apparent that further analysis was required to fully understand such a system. Because AACVD is carried out at ambient pressure, access to the deposition chamber is convenient allowing, with an altered experimental setup, the study of thin film growth over time. In this study we present the first characterisation of a thin film throughout its growth utilising *time resolved* AACVD (trAACVD) to provide further insight into the growth of a TiO_2/ SnO_2 system whilst also permitting the tracking of functional properties and post deposition tuning of properties by varying the subsequent deposition time.

Experimental

Thin film Preparation using AACVD

Nitrogen (99.99%) (BOC) was used as supplied. Depositions were obtained on SiO2 coated float-glass. Prior to use the glass substrates were cleaned using water, isopropanol and acetone and dried in air. Glass substrates of ca. 45 mm x 5 mm x 4 mm were used. The precursors, titanium tetra-iso-propoxide (99%) and tin butyl tri-chloride (99%) were obtained from Sigma-Aldrich Chemical Co. and used as supplied. Aerosols were generated in ethyl acetate (99%) and carried into the reactor in a stream of nitrogen gas through a brass baffle to obtain a laminar flow. A graphite block, containing a Whatmann cartridge heater, was used to heat the glass substrate. The temperature of the substrate was monitored using a Pt–Rh thermocouple. Depositions were carried out by heating the horizontal bed reactor to the required temperature of 450 oC before diverting the nitrogen line through the aerosol and hence to the reactor. The total time for the deposition process took 20- 25 minutes. At the end of the deposition, under the nitrogen flow, the glass substrates were left to cool to room temperature with the graphite block before it was removed. To modify the experiment to provide a time resolved study a chemically inert cover, a thin graphite foil was inserted via the exhaust into the reactor and withdrawn at specific time intervals to achieve areas of glass of differing deposition times. Initially the cover only revealed a small area of glass on which deposition can take place. By doing this eight samples can be generated in a single deposition.

Sample Characterisation

X-ray diffraction (XRD) was carried out using a Lynx-Eye Bruker X-ray diffractometer with a mono-chromated Cu Kα (1.5406 Å) source. X-ray photoelectron spectroscopy (XPS) was carried out using a Thermo Scientifiic K-Alpha instrument with monochromatic Al-Kα source to identify the oxidation state and chemical constituents. High resolution scans were done for the Ti (3d), Sn (3d), O (1s) and C (1s) at a pass energy of 40 eV. The peaks were modelled using Casa XPS software with binding energies adjusted to adventitious carbon (284.5 eV). SEM images were taken on a JOEL JSM-6301F Field Emission instrument with acceleration voltage of 5 kV. Images were captured using SEMAfore software. Samples were cut into coupons representing the different timed samples and coated with a fine layer of gold to avoid charging. The optical transmission was measured over 320–800 nm range using a Lamda 950 UV/Vis spectrometer. Film thickness was calculated using a Filmetrics F20 thin-film analyser.

Functional Property Testing

Photocatalytic activity was assessed using an established method based on a resazurin 'intelligent ink' first developed by Mills et al. [26] Photo induced wettability was tested by placing the samples under a UVC lamp for 2 hours then measuring the water contact angle by placing a 5 μL droplet onto the surface of the films. The film was then irradiated overnight for 24 hours and water contact angles were re-measured. Two point resistivity measurements were undertaken with a multimeter. Water droplet contact angles were measured using a First Ten angstroms 1000 device with a side mounted rapid fire camera after casting a 5 μL droplet from a fixed height onto the surface. To assess the photocatalytic activity of the films the samples were washed with water, rinsed with isopropanol and irradiated for 30 minutes to clean and activate the sample. A resazurin based ink was then evenly applied using a spray gun and the photo-induced degradation of the resazurin ink monitored by UV-Vis spectroscopy. Formal quantum efficiency and the formal quantum yield was then calculated. Formal quantum efficiency was calculated by dividing the rate of dye molecules destroyed per s per cm2 by the photon flux (4.53 x 1014 photons per cm^2 per s). The formal quantum yield (FQY) was calculated by dividing the rate of dye molecules destroyed per s per cm2 by the number of photons absorbed by the films. The photon flux and photon absorption for each film was determined using a UVX digital radiometer with a detector for 365 nm radiation attached.

Preparation of 'intelligent ink' solution

Glycerol (99.6%), hydroxy ethyl cellulose [average Mv ¼ 90 000], Resazurin (92%) were all purchased from Sigma-Aldrich Chemical Co. and used as supplied. The 'intelligent' ink consisted of Resazurin (40 mg) redox dye in an aqueous solution (40 mL) with glycerol (3 g) and hydroxylethyl cellulose (0.45 g) that was aged for 24 hours at 3–5 ^oC. The solution was mixed thoroughly before use.

Results

Titanium isopropoxide and butyl tin trichloride were dissolved in ethyl acetate in a 1:1 ratio and used as precursors for the deposition of a TiO_2/ SnO_2 composite material by AACVD at 450 ^oC on a glass substrate. The experimental setup allowed for the production of samples representing different deposition times. This generated seven snapshots of materials representing differing deposition times on a single substrate, which would normally require seven separate depositions. The time resolved samples were generated by withdrawing a cover across the surface of the glass at specific time intervals revealing areas of uncoated glass throughout the deposition process (**Figure 1**). The samples were characterised and their functional properties mapped.

Characterisation

The average time for a full deposition, where the aerosol source was exhausted, was shown to be between 20 and 25 minutes for 20 mls of ethyl acetate at a carrier gas flow rate of 1l/min. It was found that up to 7 areas representing different deposition times could be deposited. The time interval for depositions was set at 3 minutes. The samples were allowed to cool under nitrogen to room temperature and the structural changes characterised using X-ray diffraction (XRD), X-ray photoelectron spectroscopy (XPS), scanning electron

Figure 1: A.) Image of final deposited film with labelled timed segments cut into segments for characterisation. Films were deposited by AACVD at 450 °C under N_2 gas flow of 1l/min using titanium isopropoxide and butyl tin trichloride dissolved in ethyl acetate in the same flask. The gradation of film thickness is apparent from the least deposited sample (3 minutes) to the most deposited sample (21 minutes) initially verifying on a visual level the principle of the experiment. B.) Images i), ii) and iii) demonstrate the process of how the cover is removed every 3 minutes to reveal fresh clear areas of glass upon which deposition can take place, creating sequential areas across the whole deposition. For example in image i) an initial area of glass is left to provide the sample with the longest deposition time. ii) After 3 minutes the cover is withdrawn a set distance via the exhaust to reveal the next sample and the process is repeated until the deposition is finished. The observance and continuation of an interference pattern, characteristic of the build-up of individual layers, throughout all samples despite the presence of a cover at varying points throughout the deposition indicates that the cover does not hamper or impinge on overall flow dynamics and film formation.

microscopy (SEM) and UV-Visible spectroscopy. Changes in functional properties across the samples were followed by photo-activity measurements using a resazurin based 'intelligent ink' and photo-induced wettability studies.[26]

Figure 2: XRD patterns of films deposited at 450 °C by AACVD using titanium isopropoxide and butyl tin trichloride. Peaks denoted with C correlate with cassiterite SnO_2 phases. All other peaks are anatase TiO_2 (A). It is apparent that very little in the way of crystalline material exists at 3 minutes but crystalline material representing anatase TiO_2 appears after 6 minutes and continues to grow in prominence throughout the rest of the deposition. Cassiterite SnO_2 only appears after 18 minutes and continues to increase in peak intensity until at 21 minutes cassiterite SnO_2 peaks and anatase TiO_2 peaks exist concurrently.

XRD

X-ray diffraction was undertaken for all samples (**Figure 2**) to provide an insight into how the crystal structure of the material evolved over time. It was apparent that both anatase TiO_2 and cassiterite SnO_2 phases are present at different points in time throughout the deposition process. In the first nine minutes the formation of an anatase TiO_2 phase was observed, which exhibited strong preferential orientation with complete suppression of the [200] plane and partial suppression of the [101] and [105] planes whilst the [004] plane was enhanced. At this time anatase TiO_2 was the only crystal phase observed. This phase continues to grow in intensity throughout the deposition process. From 18 minutes onwards cassiterite SnO_2 phases appeared, in particular the [101] and [211] planes.[24] It was evident that modifying the deposition regime, to provide samples at different deposition times, did not hamper or inhibit the growth of the material under investigation in this study. Indeed this can be seen by continuation of the contour thickness planes in Figure 1A. These are due to reflection from the film and glass producing an optical interference pattern due to minute (nm) variations in film thickness.[27]

XPS

X-ray photoelectron spectroscopy (XPS) was undertaken for all samples representing the seven time intervals to identify the elements present and their respective oxidation states. Depth profiling was conducted to profile how the tin: titanium ratio changes from the surface to the bulk within a specific film.

Figure 3: A graph comparing the Sn: Ti atomic ratio in XPS depth profiling across all timed samples formed from AACVD of titanium isopropoxide and butyl tin trichloride at 450 °C. All samples were etched for 100s, this was repeated 4 times to achieve 4 levels within the bulk. Across all samples; after 3 minutes tin concentration is high, averaging about 10 times more abundant than titanium. Six minutes into the deposition titanium levels start to increase relative to tin until after 9 minutes titanium becomes the dominant element with the ratio of Sn: Ti becoming <1. In general within the bulk Sn concentration increases relative to titanium but the ratio of Sn to Ti remains <1. After 18 minutes Sn becomes the dominant element at the surface with a Sn: Ti ratio >1.

Titanium peaks were found to match those reported for TiO_2 at 458.3 eV (Ti^{4+} $2p_{3/2}$) and 463.9 (Ti^{4+} $2p_{1/2}$) eV. Tin peaks, also matching previous literature reports for SnO_2, were found at 486.5 eV (Sn^{4+} $3d_{5/2}$) and 494.9 eV (Sn^{4+} $3d_{3/2}$).[28,29] As observed in Figure 3, after 3 minutes of deposition, tin 4+ was found to be the dominant element relative to titanium 4+ at both the surface and within the bulk. After 6 minutes of deposition time levels of tin relative to titanium decreased until after 9 minutes when the surface was observed to be tin rich compared to the bulk but the ratio of tin to titanium remained <1, with the bulk material exhibiting less tin but in concentrations significantly higher than would be expected if tin was present in a typical dopant regime. Twelve minutes of deposition time produced a very similar picture with a surface richer in tin, relative to titanium, compared to the bulk but still in minority to titanium. This general pattern was found in the sample representing 15 minutes of deposition time. After 18 minutes of deposition time the surface exhibited a tin to titanium ratio >1 whilst the bulk continued to exhibit a Sn: Ti ratio <1. The full deposition time of 21 minutes exhibited a similar profile, with a surface Sn: Ti ratio >1 with a bulk ratio <1. When cross referenced with XRD it was observed that the cassiterite SnO_2 peaks coincided with the surface Sn: Ti ratio from XPS switching from <1 to >1. This indicates that SnO_2 formation occurs at the TiO_2 surface as a result of dynamic surface segregation[25] that causes Sn^{4+} to move to the surface from the bulk, when the Sn surface concentration becomes high enough (Sn: Ti >1) SnO_2 is produced at the surface (Figure 4). Shadowing earlier reports, it was found that oxygen 1s XPS spectrums for samples representing 9 minutes onwards exhibited within the bulk characteristic lattice oxygen values at 530.1 eV which is characteristic of a Sn-O-Ti linkage. Standard oxygen values for standard TiO2 and SnO2 are also exhibited (Figure S1-7). This indicated Sn as a substitutional dopant within the anatase TiO2 matrix.30,31

Figure 4: A graph displaying Sn: Ti ratio for the surface only. There are 3 distinct areas: A) 3-6 minutes: this represents a deposited amorphous solid solution of SnO2 with traces of titanium 4+. B) 9-15 minutes: tin concentration decreases to become the minority element relative to titanium producing a solid solution of tin doped titanium dioxide. C) 18- 21 minutes: It is seen that after 18 minutes Sn becomes the majority element at the surface. This coincides with XRD which displays cassiterite SnO2 after 18 minutes. This implies that first a seed layer of amorphous SnO2 forms (A). This allows the growth of a solid solution of tin doped anatase TiO2 as seen in XRD (B). It is from this solid solution that Sn surface concentration increases enough to become the majority element at the surface forcing the growth of cassiterite SnO2 (C).

SEM

Surface morphology was investigated by scanning electron microscopy (SEM) to give an insight into how the film grows over time whilst also providing additional information relevant to understanding how the photo-activity and water contact angles change over time. After three minutes of deposition material had been deposited which displayed no overall structure (**Figure 5**). After six minutes these particles appear to continue to nucleate and grow in size whilst still displaying little to no regular structure. Nine minutes into the deposition crystallites displaying an overall regular structure were observed, hinting that the growths are starting to adopt a 2-dimensional square-like geometry. This square geometry is emulated and repeated throughout depositions representing 12, 15 and 18 minutes. Overall, both crystallite size and porosity were noted to increase with deposition time. After 21 minutes of deposition time large crystallites around 100 nm in width with a square 2D profile and pyramidal 3D profile were observed whilst retaining the porosity of previous time intervals.

Ultraviolet Visible Spectroscopy

Ultraviolet-visible absorption spectroscopy was undertaken to explore how the absorption, transmission and band gap for individual samples changed over time. Transmission data was obtained from the absorption data. It is evident from Figure S8 and S9 that the observed transmission is inversely proportional to deposition time, on a simplistic level this corroborates the observation that the film increases in thickness with deposition time. Analysis of the band gap for each timed sample was calculated using Tauc plots (Figure S10). It was evident that whilst initially the band gap is closer to the expected band gap value for cassiterite SnO_2 (3.6 eV) the values steadily decrease over time and stabilise at around 3.2 eV which is characteristic of anatase TiO_2 from 12 minutes onwards. Lack of cassiterite SnO_2 peaks in the XRD at these early time intervals (3-9 minutes) suggests that these high values are due to film thickness and the resulting limitations of Tauc plot analysis for extremely thin films. This is highlighted in SEM where significantly altered film morphology was not seen to occur until 9 minutes into the deposition. By comparing band gap values with absorption and transmission data it can be concluded that because band gap values do not change over time once stabilising at 3.2 eV the apparent red-shifting observed in the absorption data can be attributed to increasing film thickness.

Film Thickness

Film thickness measurements were obtained using the Swanepoel method to gain an insight into how thickness progresses throughout the deposition. It was demonstrated that film thickness increased proportionally with deposition time in a linear fashion (Figure S11). This indicates that the stream of precursor is roughly constant throughout the deposition process until the aerosol source is exhausted.

Functional Properties

Photo-activity

Photo-activity measurements were obtained for all samples using a resazurin based 'intelligent ink'. This allowed for the rate of photo-activity to be tracked throughout the deposition process. It was found that all samples exhibited different rates of photo-activity and that these changed in relative intensity throughout the deposition process (Figure 6 i).) hinting that changes in structure and morphology may be responsible for this change in function. Formal quantum efficiency (FQE - the amount of dye molecules destroyed per incident photon) and formal quantum yield (FQY - amount of dye molecules destroyed per absorbed photon), which provide a quantitative measure of a samples ability and efficiency to absorb light, was found however to mirror and track with changes in rates of photo-activity across all samples (Figure 6 ii).).

It was apparent that photo-activity altered dramatically throughout the deposition process. Photo-activity remains low from 3- 6 minutes but then proceeds to increase substantially until 15 minutes where activity proceeds to decline until the full deposition time is reached at 21 minutes. Therefore a 'state' of enhanced photo-activity exists that would not be achieved in a traditional deposition regime and thus would not be identified otherwise.

Throughout the deposition process FQE and FQY remain separated from each other, signalling that the films photo-activity changes in intensity regardless of the films efficiency in absorbing UV photons. Contrastingly, at 21 minutes FQE and FQY appear to converge, signalling that a higher percentage of photons are absorbed and subsequently used in the generation of photo-electrons and holes. Therefore whilst the sample at 21 minutes exhibits lower photo-activity than samples 12- 15 it is a far more efficient photo catalyst (Figure 6 ii).).

Figure 5: A time lapse of SEM images that represent 3, 6, 9, 12, 15, 18 and 21 minutes of the deposition process. It is evident that film formation occurs after 3 minutes with evidence of granular particulate matter forming with no overall order. After 9 minutes square structures start to appear and become progressively larger as the deposition process continues in time. Eventually the morphology resembles large monolithic square based pyramids after 21 minutes.

Figure 6: i). A graph comparing photo-activity rates for all samples. It appears to start low (3-6 minutes) but then increase between 9-15 where it reaches a maximum and decreases from 15-21 minutes. This indicates that there are states which exhibit higher rates of photo-activity which would normally be inaccessible with a traditional deposition regime. ii). A graph comparing the relationship of formal quantum efficiency and formal quantum yield for each sample which charts how they change between samples and thus over time. FQE and FQY are seen to track concurrently with changes in photo-activity and converge around 21 minutes. iii). A. Water contact angles for all timed samples. All samples exhibit hydrophobic water contact angles roughly around 110°. B. Water contact angles after 24 hours of UVA (365nm) irradiation. Whilst early samples (3-12 minutes) retain similar water contact angles compared to before irradiation later samples (15-21 minutes) show a decrease in contact angle.

Water Contact Angles

Water contact angles were measured pre- and post-UVA (365 nm) irradiation to ascertain which samples exhibit photo induced wettability and how this particular functional property changes with deposition time. Images of water contact angles can be found in the supplementary information (**Figure 6 iii**)). It was found that hydrophobicity was immediately apparent from 3 minutes into the deposition process and continued to increase by roughly 10 degrees until a deposition time of 18 minutes. After 21 minutes the contact angle decreased to a similar value as 3 minutes. The samples were then irradiated under UV light (365 nm) for 24 hours. Samples were retested to determine the change, if any, in water contact angle post irradiation. It was observed that for samples representing 3-12 minutes deposition time little or no change was observed. However from 15 minutes onwards a decrease in contact angle was observed for all samples with the largest decrease in contact angle found at 18 and 21 minutes (**Table 1**). This can be attributed to a change in morphology and surface properties that occur when the Sn: Ti ratio, as observed in XPS, changes from being <1 to >1 and the observance of SnO_2 in the XRD for these samples which sequesters photo-electrons from TiO_2, preserving holes which induce surface defects which water can co-ordinate into thus changing the nature of the surface from hydrophobic to a more hydrophilic surface. The initial hydrophobicity observed for all samples is characteristic of nanoscale monolithic growths found in previous studies on a range of materials which also exhibit nanoscale (100 nm) monolithic surface morphology.[32–35] due to nanoscale monoliths present in surface morphology the surface exhibits a high degree of roughness.[36]

Table 1: Table comparing water contact angle values for all timed samples pre and post irradiation with UVA (365 nm) light.

Deposition Time/ minutes	Pre-Irradiation/ ^{o}	Post-Irradiation/ ^{o}
3	111.4	100.1
6	112.0	110.4
9	112.0	113.3
12	115.9	110.4
15	120.0	100.8
18	124.7	68.3
21	114.4	70.3

Discussion

Time resolved aerosol assisted chemical vapour deposition (trAACVD) was carried out at 450 oC under a N2 gas flow using a titanium dioxide precursor (titanium isopropoxide), a tin dioxide precursor (butyl tin trichloride) and an oxygen source (ethyl acetate) dissolved in the same flask. An altered experimental setup was utilised to cover and subsequently reveal fresh areas of glass at specific time intervals throughout the deposition. The resultant film achieved samples representing seven different deposition times whilst requiring one deposition in total. The samples were characterised and their functional properties mapped utilising high throughput screening methods. This provided for the first time, insight into the key growth phases of the material. The technique successfully reproduced the morphology and XRD structure of a TiO2/ SnO2 composite material.

X-ray diffraction has shown how the crystal structure develops over time. Initially preferentially orientated anatase TiO2 develops and remains the dominant phase throughout the deposition, with the addition of the [110], [200] and [211] cassiterite SnO2 peaks from 18 minutes onwards. XPS shows that from 3 minutes onwards titanium and tin 4+ species are found both at the surface and within the bulk for all samples. Three minutes into the deposition tin is the dominant element relative to titanium, this tin layer is amorphous as no diffraction pattern was observed in the XRD. This suggests that the formation of an amorphous tin layer early in the deposition process acts as a seed layer for the growth of the Sn doped TiO2 solid solution observed from 9 minutes onwards. For this composite material specifically, the tin to titanium ratio remains <1 at both the surface and within the bulk until 18 minutes where the surface ratio of tin to titanium becomes >1. Overall tin concentration is higher at the surface relative to the bulk regardless of its concentration relative to titanium. Oxygen 1s peaks at 530.1 eV observed within the bulk indicate that a Sn-O-Ti linkage exists within the matrix implicating Sn as a substitutional dopant.[30,31] This indicates that the mechanism for Sn migration is via substitution with Ti atoms within the TiO2 anatase lattice. SEM shows that the square pyramidal structure observed starts to grow from 9 minutes onwards and increases in size over time; this corroborates band gap analysis, where the band gap starts to decrease towards 3.2 eV and photo-activity where an increase in rate is seen to occur from 9 minutes onwards. The change in morphology seen at 18 and 21 minutes coincides with the inclusion of full cassiterite SnO2 peaks in the XRD.

Overall it is apparent from XPS and XRD that an anatase phase solid solution of (Ti/ SnO2 forms.[37] XRD displays two distinct crystal phases present within the composite (anatase TiO_2 and cassiterite SnO_2 and XPS depth profiling shows that titanium is dominant within the bulk, whilst the surface is Sn dominant. The XRD in context of XPS therefore strongly suggests a phase separation. From this it is speculated that surface segregation, facilitated by constant heating and time, which increases linearly between samples, forces tin to collect at the surface, causing the high concentrations of tin found at the surface for all samples, relative to the bulk. As all samples experience the same temperature inside the reactor, time is the only factor that can account for differences in surface Sn concentration and indeed it is found that; excluding 3-6 minutes, where amorphous SnO2 is deposited and acts as a seed layer for the composite phase that subsequently grows, samples which experience longer deposition times exhibit higher surface concentrations of Sn, relative to the bulk and other samples (Figure 7). This explains why the natural formation of a hetero-junction with bulk tin doped TiO2 and surface SnO2 is

attributed to surface segregation of tin and thus originates from within the original TiO2 matrix and is not a direct result of the deposition process. If this were the case, cassiterite SnO2 XRD peaks would be observed earlier on in the deposition process and would be independent of the surface ratio of tin to titanium found in XPS. This is highlighted in other studies in which the sintering process causes migration of tin through the anatase matrix.[38] Whilst the cause is identified in this study, the underlying principle for this migration observed remains unknown and is an area for further study. Therefore despite having equal amounts of precursor in the aerosol source, SnO2 nucleates much easier to the glass and TiO2 subsequently appears to nucleate much faster than SnO2 once the SnO2 layer has been established. Thermal migration of substitutional Sn through the TiO2 matrix over time then results in surface segregation of SnO2. This results in a composite of Sn-doped TiO2 capped by SnO2.

Figure 7: A schematic representing samples throughout the deposition process demonstrating how the position and concentration of Sn varies relative to Ti in time. A) Tin dioxide deposits preferentially over titanium dioxide within the first 3-6 minutes B) This initial SnO_2 layer is hypothesised to act as a seed layer allowing a Sn doped TiO_2 layer to develop (9-15 mins). As time progresses Sn begins to migrate to the surface as a result of heating (450 ^oC). C) This results in a higher concentration of Sn at the surface than within the bulk (seen in XPS), which is proposed to enhance surface photocatalysis as the Sn^{4+} sites at the surface act as electron sinks promoting electron lifetimes. D) As time progresses further, Sn concentration becomes so high that it is now the majority element present at the surface (Sn: Ti >1). The surface now converts from an anatase phase Sn doped TiO_2 solid solution to a cassiterite SnO_2 phase which caps the Sn doped TiO_2 solid solution phase from which it originated, this is observed in XRD from 18 minutes onwards. Photocatalysis is partially impaired by the formation of this SnO_2 layer but still displays a high rate of photocatalysis.

Ultraviolet-Visible spectroscopy demonstrates that although there was apparent red-shifting of absorption data, transmission was found to decrease proportionally with deposition time. Concordant with Tauc plot analysis, which shows that the band gap is 3.2 eV, it was evident that the apparent red-shifting could be attributed to increasing film thickness, which is observed to increase incrementally in a linear fashion with increasing deposition time.

Film thickness was observed to increase proportionally with time across all samples, with samples with longer deposition times exhibiting thicker films. This echoes analysis of XPS and XRD and changes in functional properties observed around 15-18 minutes cannot simply be attributed to the growth of the film and that changes within the film that occur as a result of surface segregation are responsible.

XPS showed that the Sn: Ti ratio switched from <1 to >1, coinciding with the appearance of cassiterite SnO_2 in the XRD, from 15 to 18 minutes can explain how the rate of photo-activity was seen to peak at 15 minutes and proceed to decrease onwards yet water contact angles exhibit the largest decrease in samples representing 18 and 21 minutes with 15 displaying intermediary behaviour transitions from hydrophobic to hydrophilic behaviour. This discrepancy in behaviour in these specific functional properties, which have their origins in the same underlying principle of photo-generated electrons and holes, is attributed to the formation of SnO_2 at the surface. The method of photo-activity quantification utilised in this report is photo-electron sensitive, hence the enhanced photo-activity observed at 15 minutes and the subsequent decrease after 18 minutes can be attributed to Sn^{4+} states, which act as electron sinks at the surface[25], shifting from molecular states existing within the TiO_2 band structure to bulk states inherent in SnO_2 band structure, this results in the sequestration of electrons into the SnO_2 conduction band and hence less electrons are available to carry out reduction of the dye at the surface. This also explains why samples representing 18 and 21 minutes exhibit the biggest change in water contact angle. This is attributed to the same principle, as the mechanism responsible for photo-induced wettability is electron hole sensitive, which creates defect sites which water molecules co-ordinate into, the sequestration of electrons results in the enhancement of electron hole lifetimes and hence enhanced surface defect production.

The sample representing 21 minutes worth of deposition time displayed FQE and FQY values which appeared to converge where all previous samples demonstrated a marked gap between FQE and FQY. This was attributed to a combination of increasing film thickness, thus a greater cross section for photon absorption and the increasing amount of SnO_2 at the surface which, by sequestering electrons through hetero-junction charge transfer, prolongs electron lifetimes and therefore minimises the recombination process. Therefore it can be deduced that the TiO_2 surface found at 15 minutes was more photoactive but was not as efficient as the sample at 21 minutes because electrons and holes are able to recombine throughout the entire medium. The sample at 21 minutes was a worse photo-catalyst because the surface was becoming more SnO_2 rich so less TiO_2 sites are available for photocatalysis but it is now able to sequester electrons at the surface and separate them from holes driving up the efficiency.

Conclusions

We have for the first time, to our knowledge, utilised trAACVD to provide an insight into the growth profile of a composite metal oxide thin film of technological interest. By varying deposition time comparison of functional and structural properties and how they change over time can identify intermediate materials which display functional properties and structure different from the final deposition time. This allows the change in intensity of functional properties relative to each other throughout the deposition sequence to be mapped and as a result the fine tuning of the material can be undertaken for a specific application where different functional properties can be utilised or maximised for specific purposes.

Acknowledgements

Thank you to Dr Ainara Garcia Gallastegui and Dr. Robert Menzel for useful discussions, Mr Kevin Reeves for assistance with SEM imaging and Mr Martin Vickers for XRD assistance. Thank you also to Pilkington NSG for the glass substrates. The

project was jointly funded by the Deanship of Scientific Research (DSR), King Abdulaziz University, Jeddah under grant no. D-5/432 and a UCL Impact scholarship. The authors therefore acknowledge the DSR and UCL with thanks for their technical and financial support.

Notes and references

[a] Materials Chemistry Research Centre, Department of Chemistry, University College London, 20 Gordon Street, London, U.K. WC1H 0AJ.
[b] The Gridiron Building, One Pancras Square, London, N1C 4AG.
[c] Chemistry Department, King Abdulaziz University, Saudi Arabia.

*Corresponding Author – c.j.carmalt@ucl.ac.uk.

Electronic Supplementary Information (ESI) available: Figures S1-11 as mentioned in the text. See DOI: 10.1039/b000000x/

1. A. Fujishima, *Nature*, 1972, **238**, 37–38.
2. A. J. Frank, N. Kopidakis, and J. Van De Lagemaat, *Coord. Chem. Rev.*, 2004, **248**, 1165–1179.
3. T. Kamegawa, R. Kido, D. Yamahana, and H. Yamashita, *Microporous Mesoporous Mater.*, 2013, **165**, 142–147.
4. W. Guo, F. Zhang, C. Lin, and Z. L. Wang, *Adv. Mater.*, 2012, **24**, 4761–4.
5. A. Duret and M. Grätzel, *J. Phys. Chem. B*, 2005, **109**, 17184–91.
6. J. Blanco-Galvez, P. Fernández-Ibáñez, and S. Malato-Rodríguez, *J. Sol. Energy Eng.*, 2007, **129**, 4.
7. Y. Li, J. Chen, J. Liu, M. Ma, W. Chen, and L. Li, *J. Environ. Sci. China*, 2010, **22**, 1290–1296.
8. a Kafizas and I. Parkin, *J. Am. Chem. Soc.*, 2011, **133**, 20458.
9. J.-M. Herrmann, *Environ. Sci. Pollut. Res. Int.*, 2012, **19**, 3655–65.
10. J. Qian, G. Cui, M. Jing, Y. Wang, M. Zhang, and J. Yang, *Int. J. Photoenergy*, 2012, **2012**, 1–6.
11. X. Ding, Z. Hong, Y. Wang, R. Lai, and M. Wei, *J. Alloys Compd.*, 2013, **550**, 475–478.
12. Z. Lai, F. Peng, Y. Wang, H. Wang, H. Yu, P. Liu, and H. Zhao, *J. Mater. Chem.*, 2012, **22**, 23906.
13. K. Choy, *Prog. Mater. Sci.*, 2003, **48**, 57–170.
14. M. Sato, H. Hara, T. Nishide, and Y. Sawada, *J. Mater. Chem.*, 1996, **6**, 1767.
15. C. E. Knapp, A. Kafizas, I. P. Parkin, and C. J. Carmalt, *J. Mater. Chem.*, 2011, **21**, 12644.
16. D. S. Bhachu, G. Sankar, and I. P. Parkin, *Chem. Mater.*, 2012, **24**, 4704–4710.
17. N. Noor and I. P. Parkin, *Thin Solid Films*, 2013, **532**, 26–30.
18. P. Marchand, I. Hassan, I. P. Parkin, and C. J. Carmalt, *Dalton Trans.*, 2013, **42**, 9406–22.
19. N. Noor and I. P. Parkin, *J. Mater. Chem. C*, 2013, **1**, 984.
20. J. Yoon, H. K. Oh, and Y. J. Kwag, *J. Korean Phys. Soc.*, 1998, **33**, 699–704.
21. S. M. Ali, S. T. Hussain, S. A. Bakar, J. Muhammad, and N. U. Rehman, *J. Phys. Conf. Ser.*, 2013, **439**, 012013.
22. C. Edusi, G. Sankar, and I. P. Parkin, *Chem. Vap. Depos.*, 2012, **18**, 126–132.
23. S. Sathasivam, A. Kafizas, S. Ponja, N. Chadwick, D. S. Bhachu, S. M. Bawaked, A. Y. Obaid, S. Al-Thabaiti, S. N. Basahel, C. J. Carmalt, and I. P. Parkin, *Chem. Vap. Depos.*, 2014, **20**, 69–79.
24. S. Ponja, S. Sathasivam, N. Chadwick, A. Kafizas, S. M. Bawaked, A. Y. Obaid, S. Al-Thabaiti, S. N. Basahel, I. P. Parkin, and C. J. Carmalt, *J. Mater. Chem. A*, 2013, **1**, 6271.
25. F. E. Oropeza, B. Davies, R. G. Palgrave, and R. G. Egdell, *Phys. Chem. Chem. Phys.*, 2011, **13**, 7882–91.
26. A. Mills, J. Wang, S.-K. Lee, and M. Simonsen, *Chem. Commun. (Camb).*, 2005, 2721–3.
27. R. Swanepoel, *J. Phys. E.*, 1983, **1214**.
28. H.-J. Wang and S.-C. Lee, *Mater. Trans.*, 2009, **50**, 2329–2334.
29. V. B. Kamble and A. M. Umarji, *AIP Adv.*, 2013, **3**, 082120.
30. H. B. Jiang, J. Xing, Z. P. Chen, F. Tian, Q. Cuan, X.-Q. Gong, and H. G. Yang, *Catal. Today*, 2014, **225**, 18–23.
31. J. Li and H. C. Zeng, *J. Am. Chem. Soc.*, 2007, **129**, 15839–47.
32. Z. Lin, J. Wang, X. Yin, X. Tan, R. Yu, J. Zheng, L. Zhang, and G. Chen, *Electrophoresis*, 2014, **35**, 1947–55.
33. B. Garipcan, J. Winters, J. S. Atchison, M. D. Cathell, J. D. Schiffman, O. D. Leaffer, S. S. Nonnenmann, C. L. Schauer, E. Pişkin, B. Nabet, and J. E. Spanier, *Langmuir*, 2008, **24**, 8944–9.
34. X.-M. Bao, J.-F. Cui, H.-X. Sun, W.-D. Liang, Z.-Q. Zhu, J. An, B.-P. Yang, P.-Q. La, and A. Li, *Appl. Surf. Sci.*, 2014, **303**, 473–480.
35. S. Balachandran, S. G. Praveen, R. Velmurugan, and M. Swaminathan, *RSC Adv.*, 2014, **4**, 4353.
36. D. Whitehouse, *Surfaces and their Measurements*, 2012.
37. L. Trotochaud and S. W. Boettcher, *Chem. Mater.*, 2011, **23**, 4920–4930.
38. C. Andrei, T. O'Reilly, and D. Zerulla, *Phys. Chem. Chem. Phys.*, 2010, **12**, 7241–5.

Textual and Graphical Abstract

Time resolved analysis of a thin film has allowed, for the first time, analysis of how thin film growth occurs and changes over time by aerosol assisted CVD. The generation of representative samples at different times during the deposition sequence permitted changes in crystal structure, relative concentrations of atoms, and surface morphology to be linked intrinsically to changes in functional properties.

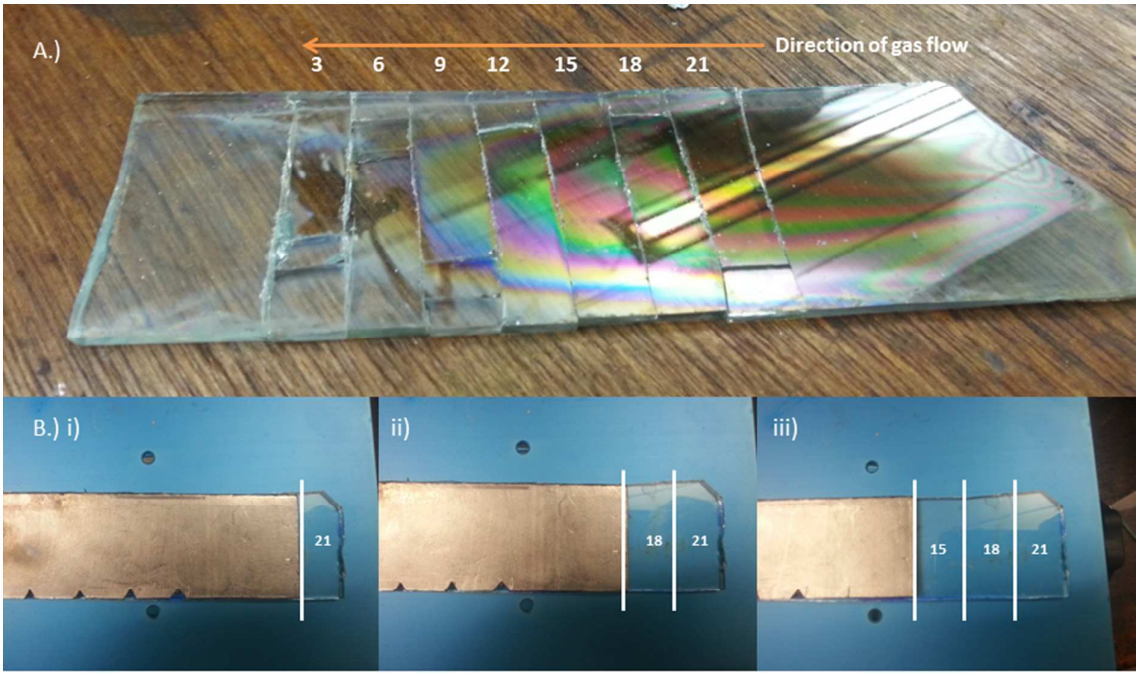

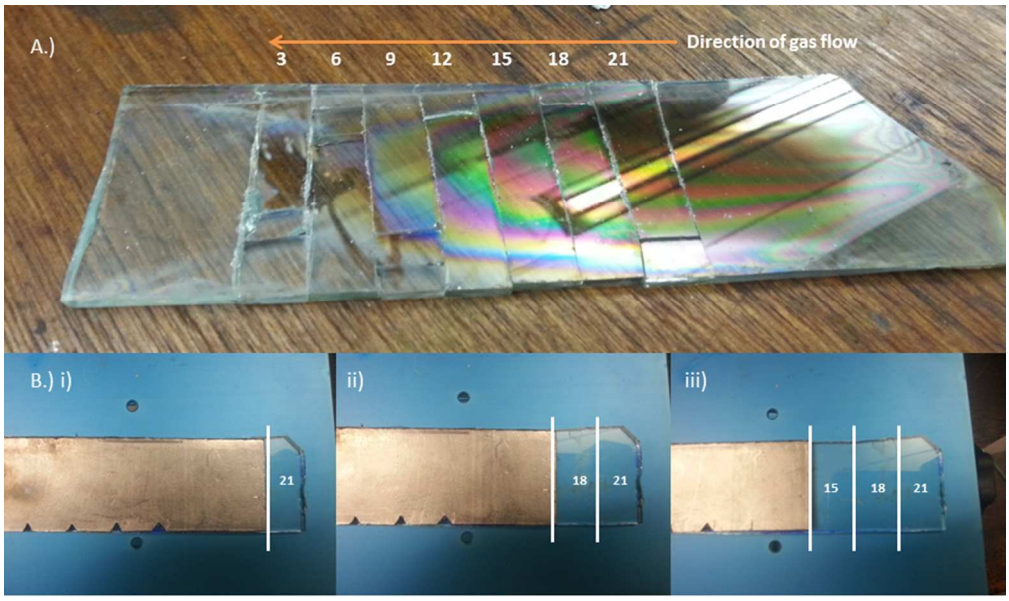

Figure 1: A.) Image of final deposited film with labelled timed segments cut into segments for characterisation. Films were deposited by AACVD at 450 ^{o}C under N_2 gas flow of 1l/min using titanium isopropoxide and butyl tin trichloride dissolved in ethyl acetate in the same flask. The gradation of film thickness is apparent from the least deposited sample (3 minutes) to the most deposited sample (21 minutes) initially verifying on a visual level the principle of the experiment. B.) Images i), ii) and iii) demonstrate the process of how the cover is removed every 3 minutes to reveal fresh clear areas of glass upon which deposition can take place, creating sequential areas across the whole deposition. For example in image i) an initial area of glass is left to provide the sample with the longest deposition time. ii) After 3 minutes the cover is withdrawn a set distance via the exhaust to reveal the next sample and the process is repeated until the deposition is finished. The observance and continuation of an interference pattern, characteristic of the build-up of individual layers, throughout all samples despite the presence of a cover at varying points throughout the deposition indicates that the cover does not hamper or impinge on overall flow dynamics and film formation.

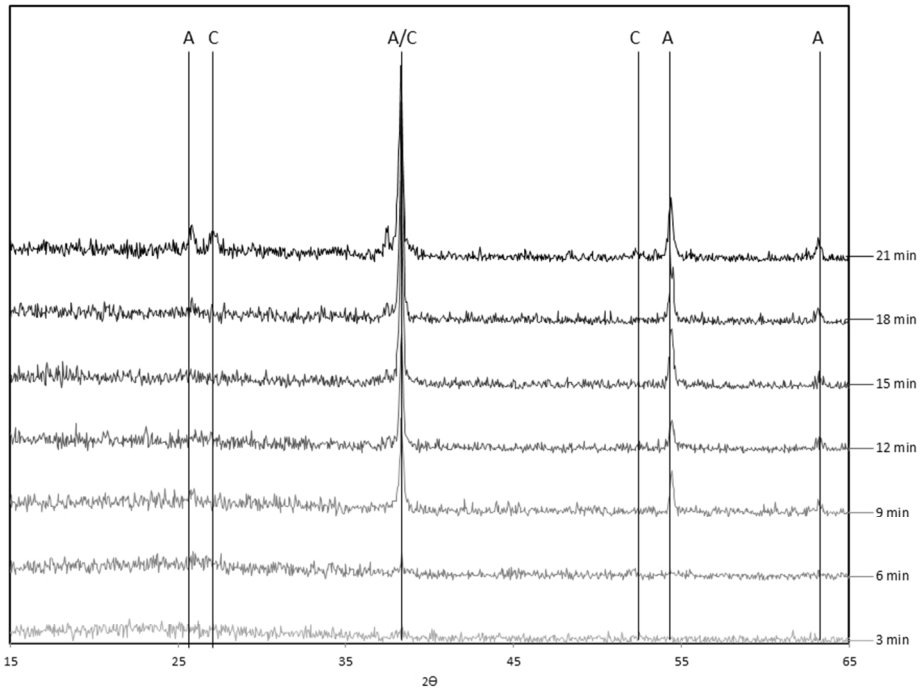

Figure 2: XRD patterns of films deposited at 450 ^{o}C by AACVD using titanium isopropoxide and butyl tin trichloride. Peaks denoted with C correlate with cassiterite SnO_2 phases. All other peaks are anatase TiO_2 (A). It is apparent that very little in the way of crystalline material exists at 3 minutes but crystalline material representing anatase TiO_2 appears after 6 minutes and continues to grow in prominence throughout the rest of the deposition. Cassiterite SnO_2 only appears after 18 minutes and continues to increase in peak intensity until at 21 minutes cassiterite SnO_2 peaks and anatase TiO_2 peaks exist concurrently.

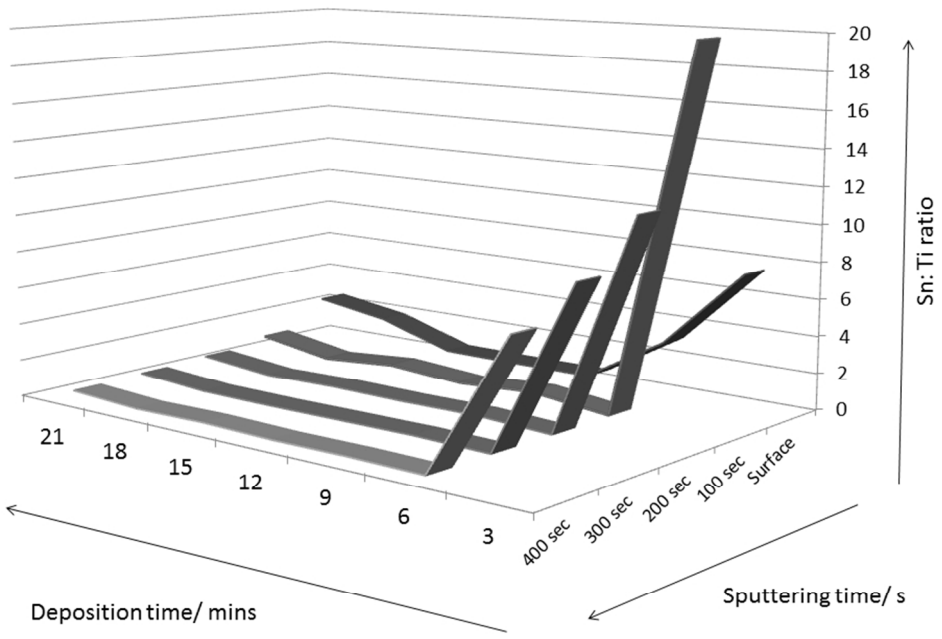

Figure 3: A graph comparing the Sn: Ti atomic ratio in XPS depth profiling across all timed samples formed from AACVD of titanium isopropoxide and butyl tin trichloride at 450 ^{o}C. All samples were etched for 100s, this was repeated 4 times to achieve 4 levels within the bulk. Across all samples; after 3 minutes tin concentration is high, averaging about 10 times more abundant than titanium. Six minutes into the deposition titanium levels start to increase relative to tin until after 9 minutes titanium becomes the dominant element with the ratio of Sn: Ti becoming <1. In general within the bulk Sn concentration increases relative to titanium but the ratio of Sn to Ti remains <1. After 18 minutes Sn becomes the dominant element at the surface with a Sn: Ti ratio >1.

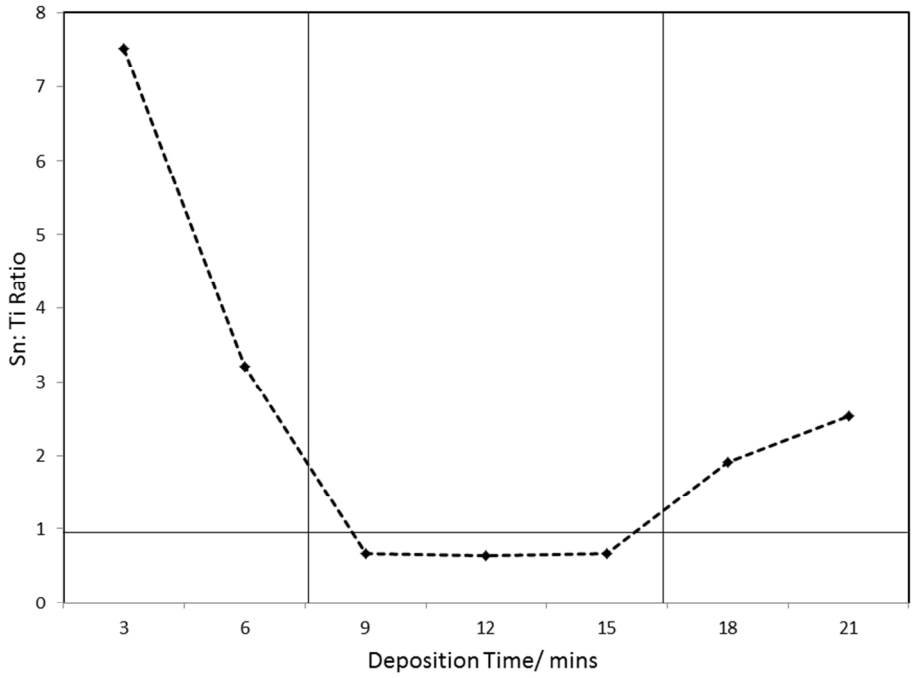

Figure 4: A graph displaying Sn: Ti ratio for the surface only. There are 3 distinct areas: A) 3-6 minutes: this represents a deposited amorphous solid solution of SnO_2 with traces of titanium 4+. B) 9-15 minutes: tin concentration decreases to become the minority element relative to titanium producing a solid solution of tin doped titanium dioxide. C) 18- 21 minutes: It is seen that after 18 minutes Sn becomes the majority element at the surface. This coincides with XRD which displays cassiterite SnO_2 after 18 minutes. This implies that first a seed layer of amorphous SnO_2 forms (A). This allows the growth of a solid solution of tin doped anatase TiO_2 as seen in XRD (B). It is from this solid solution that Sn surface concentration increases enough to become the majority element at the surface forcing the growth of cassiterite SnO_2 (C).

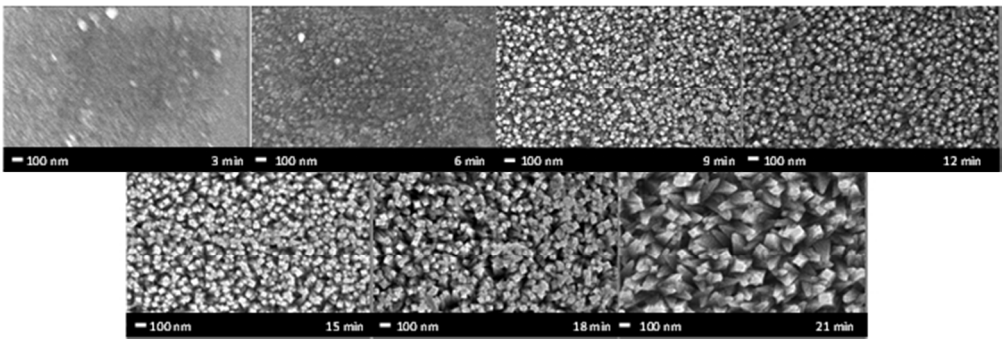

Figure 5: A time lapse of SEM images that represent 3, 6, 9, 12, 15, 18 and 21 minutes of the deposition process. It is evident that film formation occurs after 3 minutes with evidence of granular particulate matter forming with no overall order. After 9 minutes square structures start to appear and become progressively larger as the deposition process continues in time. Eventually the morphology resembles large monolithic square based pyramids after 21 minutes.

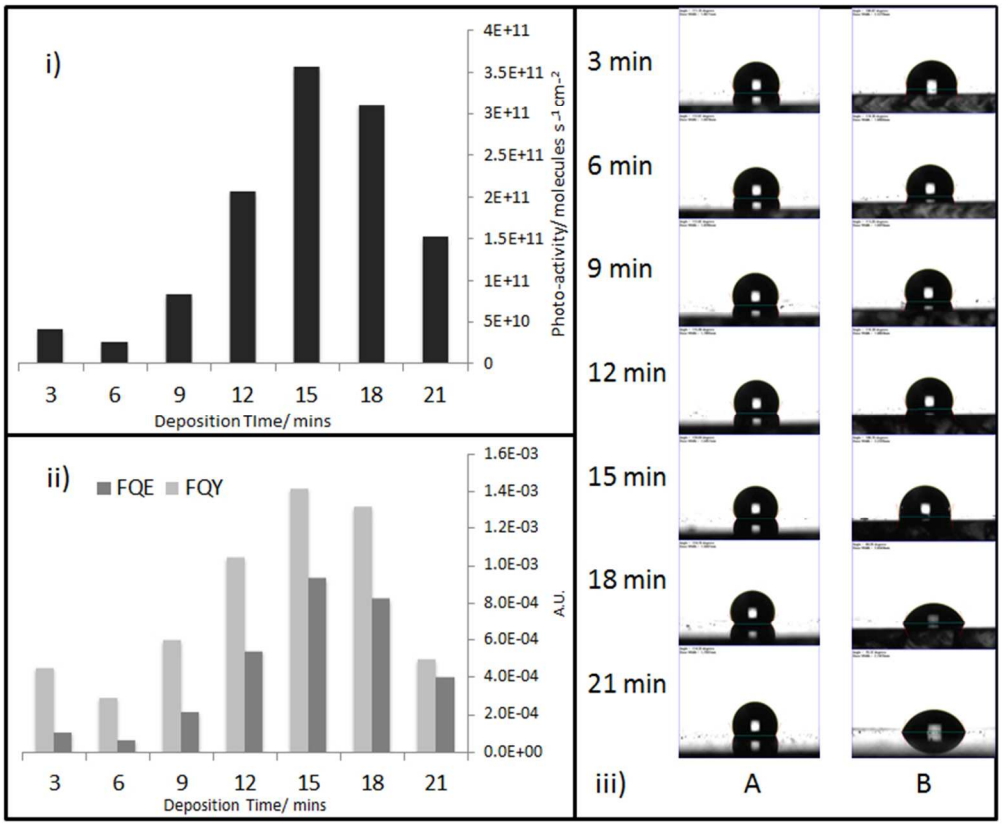

Figure 6: i). A graph comparing photo-activity rates for all samples. It appears to start low (3-6 minutes) but then increase between 9-15 where it reaches a maximum and decreases from 15-21 minutes. This indicates that there are states which exhibit higher rates of photo-activity which would normally be inaccessible with a traditional deposition regime. ii). A graph comparing the relationship of formal quantum efficiency and formal quantum yield for each sample which charts how they change between samples and thus over time. FQE and FQY are seen to track concurrently with changes in photo-activity and converge around 21 minutes. iii). A. Water contact angles for all timed samples. All samples exhibit hydrophobic water contact angles roughly around 110°. B. Water contact angles after 24 hours of UVA (365nm) irradiation. Whilst early samples (3-12 minutes) retain similar water contact angles compared to before irradiation later samples (15-21 minutes) show a decrease in contact angle.

Deposition Time/ minutes	Pre-Irradiation/ °	Post-Irradiation/ °
3	111.4	100.1
6	112.0	110.4
9	112.0	113.3
12	115.9	110.4
15	120.0	100.8
18	124.7	68.3
21	114.4	70.3

Table 1: Table comparing water contact angle values for all timed samples pre and post irradiation with UVA (365 nm) light.

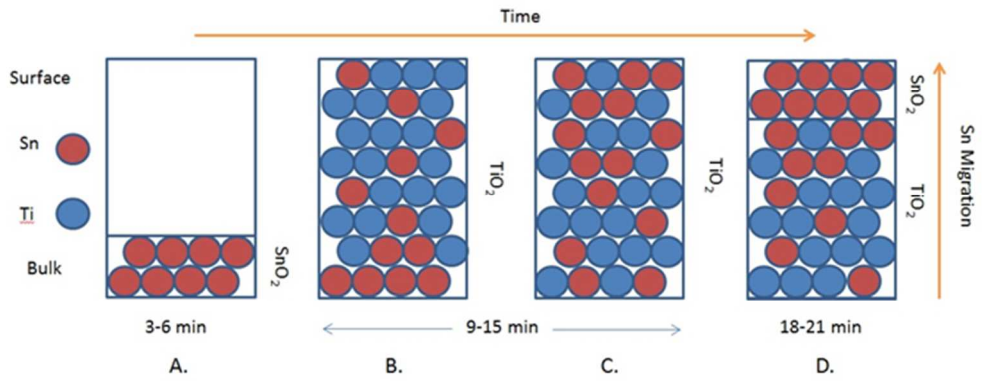

Figure 7: A schematic representing samples throughout the deposition process demonstrating how the position and concentration of Sn varies relative to Ti in time. A) Tin dioxide deposits preferentially over titanium dioxide within the first 3-6 minutes B) This initial SnO_2 layer is hypothesised to act as a seed layer allowing a Sn doped TiO_2 layer to develop (9-15 mins). As time progresses Sn begins to migrate to the surface as a result of heating (450 ^{o}C). C) This results in a higher concentration of Sn at the surface than within the bulk (seen in XPS), which is proposed to enhance surface photocatalysis as the Sn4+ sites at the surface act as electron sinks promoting electron lifetimes. D) As time progresses further, Sn concentration becomes so high that it is now the majority element present at the surface (Sn: Ti >1). The surface now converts from an anatase phase Sn doped TiO_2 solid solution to a cassiterite SnO_2 phase which caps the Sn doped TiO_2 solid solution phase from which it originated, this is observed in XRD from 18 minutes onwards. Photocatalysis is partially impaired by the formation of this SnO_2 layer but still displays a high rate of photocatalysis.